Equilibrium and Kinetics of the Folding and Unfolding of Canine Milk Lysozyme †

ARTICLE *in* BIOCHEMISTRY · JUNE 2007

Impact Factor: 3.02 · DOI: 10.1021/bi602464v · Source: PubMed

Equilibrium and Kinetics of the Folding and Unfolding of Canine Milk Lysozyme†

Hiroyasu Nakatani,‡ Kosuke Maki,§ Kimiko Saeki,§ Tomoyasu Aizawa,|| Makoto Demura,⊥ Keiichi Kawano,|| Shuji Tomoda,‡ and Kunihiro Kuwajima*,§,#

Department of Life Science, Graduate School of Arts and Sciences, University of Tokyo, 3-8-1 Komaba, Meguro-ku, Tokyo 153-8902, Japan, Department of Physics, Graduate School of Science, University of Tokyo, 7-3-1 Hongo, Bunkyo-ku, Tokyo 113-0033, Japan, Division of Biological Sciences, Graduate School of Science, Hokkaido University, N10 W8 Kita-ku, Sapporo, Hokkaido 060-0810, Japan, and Bioinformatics and Molecular Science course, Graduate School of Life Science, Hokkaido University, N10 W8 Kita-ku, Sapporo, Hokkaido 060-0810, Japan

Received November 30, 2006; Revised Manuscript Received February 27, 2007

ABSTRACT: The equilibrium and kinetics of canine milk lysozyme folding/unfolding were studied by peptide and aromatic circular dichroism and tryptophan fluorescence spectroscopy. The Ca^{2+}-free apo form of the protein exhibited a three-state equilibrium unfolding, in which the molten globule state is well populated as an unfolding intermediate. A rigorous analysis of holo protein unfolding, including the data from the kinetic refolding experiments, revealed that the holo protein also underwent three-state unfolding with the same molten globule intermediate. Although the observed kinetic refolding curves of both forms were single-exponential, a burst-phase change in the peptide ellipticity was observed in both forms, and the burst-phase intermediates of both forms were identical to each other with respect to their stability, indicating that the intermediate does not bind Ca^{2+}. This intermediate was also shown to be identical to the molten globule state observed at equilibrium. The Φ-value analysis, based on the effect of Ca^{2+} on the folding and unfolding rate constants, showed that the Ca^{2+}-binding site was not yet organized in the transition state of folding. A comparison of the result with that previously reported for α-lactalbumin indicated that the folding initiation site is different between canine milk lysozyme and α-lactalbumin, and hence, the folding pathways must be different between the two proteins. These results thus provide an example of the phenomenon wherein proteins that are very homologous to each other take different folding pathways. It is also shown that the native state of the apo form is composed of at least two species that interconvert.

For more than four decades, the problem of protein folding has been one of the most important unresolved problems in biochemistry and molecular structural biology (*1*). Many globular proteins undergo reversible folding/unfolding transitions, and the detection and characterization of an intermediate species between the native and fully unfolded states have been central to experimental studies of protein folding (*2*−*4*), although it is also known that small proteins with less than 100 amino acid residues often show two-state folding transition without the detectable folding intermediate (*5*).

The molten globule (MG[1]) state has been known as an intermediate between the native (N) and fully unfolded (U) states for a number of globular proteins. This state has the following common structural characteristics (*2*−*4*): (i) the presence of a pronounced amount of secondary structure, (ii) the absence of most of the specific tertiary structure produced by tight packing of side chains, (iii) the compactness of a protein molecule with a radius 10 to 30% larger than that of the N state, and (iv) the presence of a loosely packed hydrophobic core accessible to solvent. The MG state is often observed as an equilibrium intermediate of the unfolding transition in a number of globular proteins (*2*−*4*). Studies of many proteins, including those exhibiting the equilibrium MG state, by stopped-flow circular dichroism (CD) and by a pulsed hydrogen-exchange technique combined with NMR spectroscopy, have shown that the same MG state is also observed as a transient kinetic intermediate formed at an early stage of refolding from the U state (*6*−*8*). Therefore, it has been proposed that the folding of these proteins obeys a sequential model in which the MG state transiently accumulates as an obligatory on-pathway intermediate of folding (*3*, *4*, *6*, *8*).

† This work was supported by a Grant-in-Aid for Scientific Research on Priority Areas (no. 15076201) and by a Grant-in-Aid for Scientific Research (B) (no. 17370052) from the Ministry of Education, Culture, Science, Sports and Technology (MEXT) of Japan.

* To whom correspondence should be addressed. Phone: +81-564-59-5230. Fax: +81-564-59-5234. E-mail: kuwajima@ims.ac.jp.

‡ Department of Life Science, University of Tokyo.

§ Department of Physics, University of Tokyo.

|| Division of Biological Sciences, Hokkaido University.

⊥ Bioinformatics and Molecular Science Course, Hokkaido University.

Present address: Okazaki Institute for Integrative Bioscience, National Institutes of Natural Sciences, 5-1 Higashiyama, Myodaiji, Okazaki, Aichi 444-8787, Japan.

[1] Abbreviations: MG, molten globule; α-LA, α-lactalbumin; N, the native state; U, the unfolded state; GdnHCl, guanidine hydrochloride; CD, circular dichroism; *E. coli*, *Escherichia coli*; EGTA, *O*,*O*′-bis(2-aminoethyl)ethyleneglycol-*N*,*N*,*N*′,*N*′-tetraacetic acid; UV, ultraviolet; I, the equilibrium unfolding intermediate; I_B, the burst-phase intermediate; N_F, the fast-unfolding native species; N_S, the slow-unfolding native species; AK, adenylate kinase; DHFR, dihydrofolate reductase; SNase, staphylococcal nuclease.

10.1021/bi602464v CCC: $37.00
Published on Web 04/04/2007

Canine milk lysozyme is a Ca^{2+}-binding lysozyme that contains 129 amino acid residues and has a molecular weight of 14,500 (*9*, *10*). This protein is homologous to other lysozymes and α-lactalbumin (α-LA), and hence, it is a member of the lysozyme/α-LA family (*11*, *12*). A crystallographic study has shown that the structure of canine milk lysozyme is also very similar to those of other lysozymes and α-LA (*13*). The structure of canine milk lysozyme thus consists of two domains, an α-domain and a *β*-domain divided by a deep cleft. The α-domain consists mainly of four α-helices, the A-, B-, C-, and D-helices from the N-terminal to the C-terminal side. The *β*-domain is formed by a series of loops and three antiparallel *β*-strands.

Equilibrium thermal unfolding and hydrogen-exchange studies have shown that recombinant canine milk lysozyme exhibits an intermediate that has the characteristics of the MG state (*13*−*15*). The MG intermediate of canine milk lysozyme was also observed in the equilibrium unfolding induced by guanidine hydrochloride (GdnHCl) (*10*, *16*, *17*). The MG state of this protein is more stable and more native-like than the classic MG state of other lysozymes and α-LA because the MG state of the canine protein partly retains specific tertiary packing structures of aromatic side chains (*15*, *16*). Although equine milk lysozyme, another Ca^{2+}-binding lysozyme, also exhibits a similar native-like MG state, the MG state of the canine protein is even more stable and more native-like. Indeed the stability of the canine protein's MG state is highest among the members of the lysozyme/α-LA family.

Kinetic refolding from the GdnHCl-induced U state was studied in authentic lysozyme prepared from canine milk as well as in the recombinant protein expressed by *Escherichia coli* (*E. coli*). In both cases, the so-called burst-phase intermediate accumulated as a kinetic folding intermediate (*17*, *18*). However, the relationship between the equilibrium MG state and the kinetic burst-phase intermediate of folding has not been fully understood in canine milk lysozyme. Furthermore, the effect of Ca^{2+} on the equilibrium and kinetics of folding/unfolding has not been quantitatively analyzed, although it is known that Ca^{2+} has a large effect on equilibrium unfolding but a marginal effect on kinetic refolding (*17*). Because the characteristics of the MG state of canine milk lysozyme are distinctive in stability and native-like structure, the characterization of the folding/unfolding reactions of this protein may provide a key to understanding possible general folding mechanisms of the proteins in the lysozyme/α-LA family.

In this study, we have investigated the GdnHCl-induced equilibrium unfolding of canine milk lysozyme by CD and fluorescence spectroscopy, and the kinetic unfolding and refolding by stopped-flow CD and fluorescence measurements. Because the recombinant protein expressed by *E. coli* has an extra N-terminal methionine residue that remarkably destabilizes the protein (*19*, *20*), we prepared our canine milk protein using a methylotrophic yeast *Pichia pastoris* expression system to avoid the addition of the N-terminal methionine residue. It is shown that the kinetic refolding reactions of both the apo and holo proteins are well represented by a sequential model of folding that involves the N, the intermediate, and the U states and that this kinetic folding intermediate is identical to the equilibrium MG state. On the basis of the effect of Ca^{2+} on the folding and unfolding rate constants (the Φ-value analysis), we know that the Ca^{2+}-binding site is not yet organized in the transition state of folding, indicating that the folding initiation site must be located outside the Ca^{2+}-binding site. A comparison of the result with those previously reported for bovine and goat α-LA demonstrates that canine milk lysozyme and α-LA have different folding initiation sites and hence different folding pathways in spite of their structural similarity. Finally, it has also been found that the N state of the apo form is heterogeneous and composed of at least two native species that interconvert with a rate constant on the order of 1 s^{-1}.

MATERIALS AND METHODS

Materials. We followed the procedures of Akieda et al. (*21*) to express the recombinant wild-type and the N49D variant of canine milk lysozyme using a *Pichia pastoris* expression system. To avoid N-linked glycosylation with this yeast expression system, an aspartyl (Asp) residue was substituted for Asn49, one of the residues of the potential glycosylation sites. This substitution was chosen because Asn49 is exposed to solvent in the N state so that this site may be easiest to glycosylate. GdnHCl was a specially prepared reagent grade and was obtained from Nacalai Tesque, Inc. (Kyoto, Japan). All other chemicals were of guaranteed reagent grade. The concentration (*c*) of GdnHCl was determined by an Atago 3T Abbe refractometer using the following equation at 589.3 nm (*22*):

$$c = 57.147(\Delta N) + 38.68(\Delta N)^2 - 91.60(\Delta N)^3 \quad (1)$$

where ΔN is the refractive index increment at 20 °C. The concentrations of the wild-type and the N49D variant of canine milk lysozyme were spectrophotometrically determined at 280 nm with an extinction coefficient of 3.36×10^4 M^{-1} cm^{-1} (*10*).

Equilibrium Measurements. Equilibrium CD and fluorescence measurements were carried out in a Jasco J-720 spectropolarimeter and a Jasco FP-777 spectrofluorometer (Tokyo, Japan), respectively. The protein samples for the measurements were prepared in 50 mM sodium cacodylate buffer (pH 7.0) that contained 50 mM NaCl, 10 mM $CaCl_2$ (the holo form), or 2 mM *O*,*O*′-bis(2-aminoethyl)ethyleneglycol-*N*,*N*,*N*′,*N*′-tetraacetic acid (EGTA) (the apo form), and an indicated concentration of GdnHCl. The path length of the cuvette was 1.0 mm for the far-UV CD measurements and 10.0 mm for the near-UV CD and fluorescence measurements. The temperature of the sample solution was controlled by circulating water at 25 °C. The protein concentration was 5.8−5.9 *μ*M for the CD measurements and 2.8−2.9 *μ*M for the fluorescence measurements.

Kinetic Measurements. Kinetic CD measurements were carried out using a stopped-flow apparatus (specially constructed by Unisoku, Inc., Osaka, Japan) attached to the Jasco J-720 spectropolarimeter. In all of the kinetic experiments, the solutions used contained 50 mM sodium cacodylate and 50 mM NaCl at pH 7.0. The temperature in the apparatus was maintained at 25 °C by circulating water.

In refolding experiments, the protein solution prepared in the sodium cacodylate buffer that contained 10 mM $CaCl_2$ and 8.2 M GdnHCl (the holo form) or 2 mM EGTA and 7.9 M GdnHCl (the apo form) were mixed with the refolding buffer (the sodium cacodylate buffer that contained 10 mM

$CaCl_2$ (the holo form) or 2 mM EGTA (the apo form), and an appropriate concentration of GdnHCl) with a mixing ratio of 1:10.3 (the protein solution)/(the diluent)).

In unfolding experiments, the native proteins in the sodium cacodylate buffer that contained 10 mM $CaCl_2$ (the holo form) or 2 mM EGTA (the apo form) were mixed with the unfolding buffer (the sodium cacodylate buffer that contained 10 mM $CaCl_2$ (the holo form) or 2 mM EGTA (the apo form) and an appropriate concentration of GdnHCl). The dead time of the stopped-flow measurements was 25 ms, and the instrumental response time of the CD spectropolarimeter was about 15 ms. The final protein concentration was 5.0−5.5 μM.

The fluorescence kinetics for refolding and unfolding were measured using an SX.18MV stopped-flow fluorescence apparatus (Applied PhotoPhysics, Leatherhead, U.K.). The excitation was at 295 nm, and fluorescence emission was observed around 350 nm using a band-pass filter (U-350, Hoya Co., Japan). In unfolding experiments, the native N49D variant in sodium cacodylate buffer containing 2 mM EGTA was mixed with unfolding sodium cacodylate buffer containing 2 mM EGTA and 7.9 M GdnHCl with a mixing ratio of 1:5 ((the protein solution)/(the diluent)). In refolding experiments, the unfolded protein in sodium cacodylate buffer containing 2 mM EGTA and 6.6 M GdnHCl was mixed with refolding sodium cacodylate buffer containing 2 mM EGTA. The dead time of the stopped-flow apparatus was 3.5 ms, and the final protein concentration was 2.0−2.2 μM.

Double-Jump Experiment. For the double-jump interrupted unfolding, the native N49D variant in sodium cacodylate buffer containing 2 mM EGTA was first unfolded by mixing with unfolding sodium cacodylate buffer containing 2 mM EGTA and 7.2 M GdnHCl in the SX.18MV stopped-flow fluorescence apparatus. After various aging times, the second mixing with refolding sodium cacodylate buffer containing 2 mM EGTA interrupted further unfolding and refolded the already unfolded protein. The final concentrations of GdnHCl and the protein were 1.1 M and 1.3 μM, respectively.

Mass Spectrometry and N-Terminal Amino Acid Sequence Analysis. Because all the arguments in this article are based on the assumption that the N49D variant used in the present study is chemically homogeneous, this was tested by mass spectrometric and N-terminal amino acid sequence analyses.

Mass spectra of our purified protein were measured by APRO Science, Inc. (Naruto, Tokushima, Japan) using MALDI-TOF-MASS with an Applied Biosystems model Voyager-DE STR mass spectrometer. Sinapinic acid was used as the matrix, and insulin and apomyoglobin were used as standard proteins to calibrate the mass axis (m/z). From the mass spectrometric analysis, there was only a single major peak with a mass of 14469.5 ± 1.1, which was identical to the mass (14470.3) of the N49D variant.

The N-terminal sequence analysis of our purified protein was also carried out by APRO Science, Inc. using a G1005A protein sequencing system (Hewlett-Packard, Palo Alto, CA). The N-terminal sequence of our purified recombinant protein was identical to that of the authentic protein, leading to the conclusion that our purified N49D variant must be chemically homogeneous.

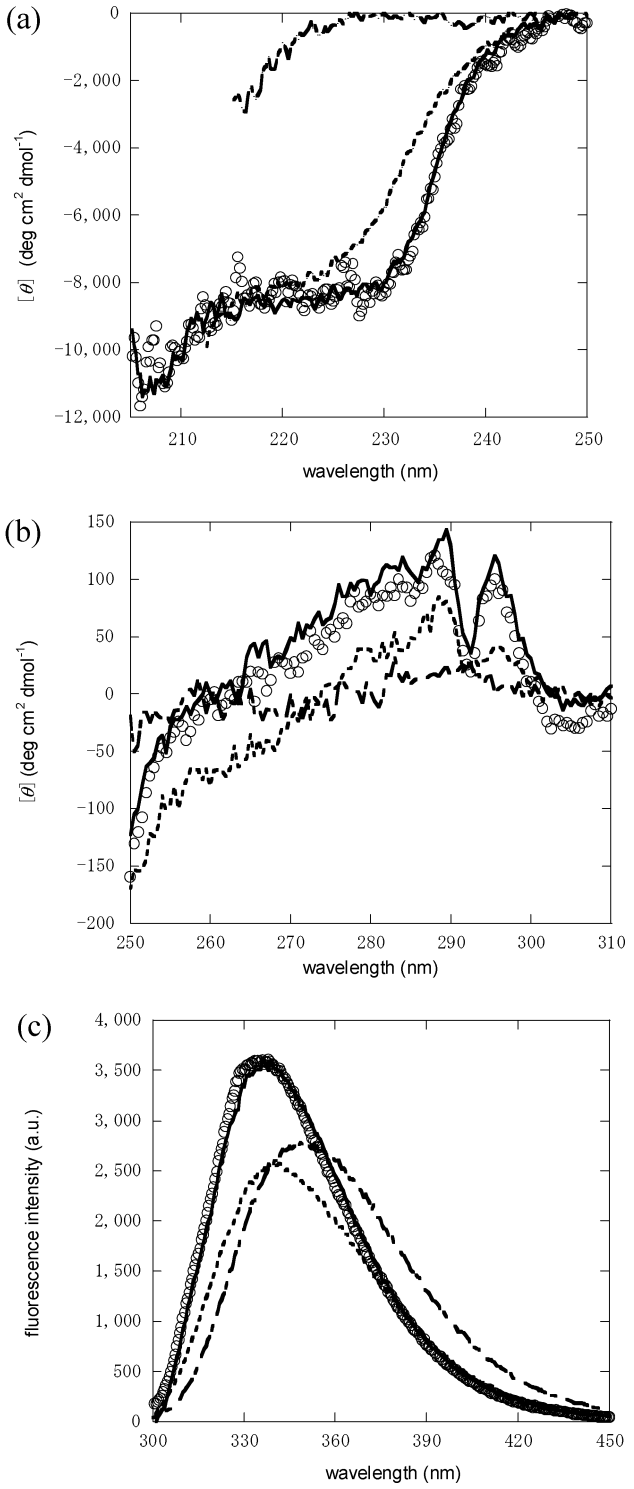

FIGURE 1: CD spectra of the holo- and apo-N49D variants (a) in the far-UV region and (b) in the near-UV region, and (c) fluorescence spectra of the holo and apo forms (pH 7.0 and 25 °C). The spectra of the holo protein in the N state (0 M GdnHCl; ○) and the apo form in the N state (0 M GdnHCl; —), I state (3.5 M GdnHCl; ····), and U state (8.0 M GdnHCl; ----) are shown.

RESULTS

CD and Fluorescence Spectra of the N49D Variant and Wild-Type Canine Milk Lysozyme. Figure 1 shows the far- and near-UV CD spectra and tryptophan fluorescence spectra of the N49D variant of canine milk lysozyme in the holo form in 10 mM $CaCl_2$ and in the apo form in 2 mM EGTA

in 50 mM sodium cacodylate plus 50 mM NaCl, at pH 7.0 and 25 °C. Hereafter, we use the terms holo and apo forms for the protein in 10 mM $CaCl_2$ and in 2 mM EGTA, respectively. Under native conditions at a low GdnHCl concentration, the holo form thus corresponds to the Ca^{2+}-bound lysozyme, whereas the apo form corresponds to the Ca^{2+}-free protein because the free Ca^{2+} concentration (<0.01 μM) in 2 mM EGTA is less than the protein concentration (2−6 μM) and the dissociation constant (>0.1 μM) for the Ca^{2+} binding to the protein. The far-UV CD spectra for the holo and apo forms at 0 M GdnHCl are coincident with each other, and both show large negative ellipticity between 205 and 230 nm, indicating the presence of α-helices. The near-UV CD spectra for the two forms at 0 M GdnHCl are coincident with each other above 290 nm, although the spectrum for the holo form is less intense below 290 nm. The spectra of the two forms thus show characteristic positive Cotton effects at 289 and 295 nm and a trough at 292 nm, indicating the presence of specific tertiary packing of aromatic side chains. The fluorescence spectra for the holo and apo forms at 0 M GdnHCl have maxima at 333 and 336 nm, respectively, and the intensity is higher for the holo form than for the apo form. The spectra at 8 M GdnHCl are coincident between the holo and apo forms, red-shifted with a maximum at 350 nm, and less intense than the spectra at 0 M GdnHCl.

We also measured the far- and near-UV CD spectra for the holo and apo forms of wild-type canine milk lysozyme at 0 and 8 M GdnHCl. They were identical to the corresponding spectra of the N49D variant (data not shown), indicating that the mutation exerted no influence on the structure in either form. These CD spectral properties are thus in reasonable agreement with those previously reported for authentic and recombinant canine milk lysozyme, the latter of which had an extra methionine residue at the N-terminus.

Equilibrium Unfolding. GdnHCl-induced equilibrium unfolding transitions of the holo and apo forms of the N49D variant were studied by CD measurements at three different wavelengths (222, 230, and 295 nm) and by measurements of integrated tryptophan fluorescence emission between 345 and 355 nm, at pH 7.0 and 25 °C. Figure 2 shows the unfolding transition curves thus obtained. In the holo form, the transition curves of the protein apparently show a single-step transition, irrespective of the spectral probes that follow the unfolding. However, transition curves of the apo form, measured by CD at 230 and 295 nm and by integrated fluorescence between 345 and 355 nm, show two transitions, indicating the presence of at least one stable unfolding intermediate. To interpret these results, we first apply a two-state unfolding model to the holo form and a three-state unfolding model, which involves a stable unfolding intermediate, to the apo form.

In the two-state model for holo N49D, only the N and the U states are populated in the transition zone as follows:

$$\mathrm{N} \overset{K_{\mathrm{NU}}}{\rightleftharpoons} \mathrm{U} \qquad \text{(scheme 1)}$$

where K_{NU} is the equilibrium constant of the unfolding reaction between N and U. Any observed quantity, $A_{obs}(c)$, (CD ellipticity or fluorescence intensity) of the protein at a GdnHCl concentration, c, is thus related to K_{NU} as follows:

$$A_{\mathrm{obs}}(c) = \frac{A_{\mathrm{N}} + A_{\mathrm{U}}K_{\mathrm{NU}}}{1 + K_{\mathrm{NU}}} = \frac{(a_{\mathrm{N}} + b_{\mathrm{N}}c) + (a_{\mathrm{U}} + b_{\mathrm{U}}c)\,K_{\mathrm{NU}}}{1 + K_{\mathrm{NU}}} \qquad (2)$$

where A_N and A_U are the observed parameter values in the pure N and pure U states, respectively, and they are assumed to be linearly dependent on c as $A_N = a_N + b_N c$ and $A_U = a_U + b_U c$. Here, the dependence of K_{NU} on c is given by (*22, 23*) the following:

$$K_{\mathrm{NU}} = \exp\left[-\left(\Delta G_{\mathrm{NU}}^{\mathrm{H_2O}} - m_{\mathrm{NU}}c\right)/RT\right] \qquad (3)$$

where $\Delta G_{NU}^{H_2O}$ is the free energy difference between the N and the U at 0 M GdnHCl, m_{NU} represents the cooperativity index of the transition, and R and T are the gas constant and the absolute temperature, respectively.

In the three-state model for apo N49D, an equilibrium unfolding intermediate (I) is stably populated during the unfolding transitions from the N to the U as follows:

$$\mathrm{N} \overset{K_{\mathrm{NI}}}{\rightleftharpoons} \mathrm{I} \overset{K_{\mathrm{IU}}}{\rightleftharpoons} \mathrm{U} \qquad \text{(scheme 2)}$$

where K_{NI} and K_{IU} are the equilibrium constants of the unfolding transitions from the N to the I and from the I to the U, respectively. It follows that

$$A_{\mathrm{obs}}(c) = \frac{A_{\mathrm{N}} + A_{\mathrm{I}}K_{\mathrm{NI}} + A_{\mathrm{U}}K_{\mathrm{NI}}\cdot K_{\mathrm{IU}}}{1 + K_{\mathrm{NI}} + K_{\mathrm{NI}}\cdot K_{\mathrm{IU}}} = \frac{(a_{\mathrm{N}} + b_{\mathrm{N}}c) + (a_{\mathrm{I}} + b_{\mathrm{I}}c)K_{\mathrm{NI}} + (a_{\mathrm{U}} + b_{\mathrm{U}}c)K_{\mathrm{NI}}\cdot K_{\mathrm{IU}}}{1 + K_{\mathrm{NI}} + K_{\mathrm{NI}}\cdot K_{\mathrm{IU}}} \qquad (4)$$

where A_N, A_I, and A_U are the observed parameter values in the pure N, pure I, and pure U states, respectively, and we again assumed the linear dependence of these parameters on c. The dependence of K_{NI} and K_{IU} on c is given by the following:

$$K_{\mathrm{NI}} = \exp\left[-\left(\Delta G_{\mathrm{NI}}^{\mathrm{H_2O}} - m_{\mathrm{NI}}c\right)/RT\right] \qquad (5)$$

$$K_{\mathrm{IU}} = \exp\left[-\left(\Delta G_{\mathrm{IU}}^{\mathrm{H_2O}} - m_{\mathrm{IU}}c\right)/RT\right] \qquad (6)$$

where $\Delta G_{NI}^{H_2O}$ and $\Delta G_{IU}^{H_2O}$ are the free energy differences between the N and the I and between the I and the U, respectively, at 0 M GdnHCl, and m_{NI} and m_{IU} represent the cooperativity indexes of the transitions from N to I and from I to U, respectively.

The data in Figure 2 were analyzed on the basis of eqs 2−6 by the nonlinear least-squares method. In this analysis, we performed global fitting, in which the transition curves were fitted simultaneously with local parameters for each transition curve and global parameters common for every transition curve. For the two-state model (the holo form), we have the four local parameters, a_N, b_N, a_U, and b_U, and the two global parameters, $\Delta G_{NU}^{H_2O}$ and m_{NU} (eqs 2−3). For the three-state model (the apo form), we have the six local parameters, a_N, b_N, a_I, b_I, a_U, and b_U, and the four global parameters $\Delta G_{NI}^{H_2O}$, $\Delta G_{IU}^{H_2O}$, m_{NI}, and m_{IU} (eqs 4−6). The thermodynamic parameters thus obtained are summarized in Table 1. The population of the I is most prevalent and at 91% at 3.4 M GdnHCl in the apo form. The solid lines in

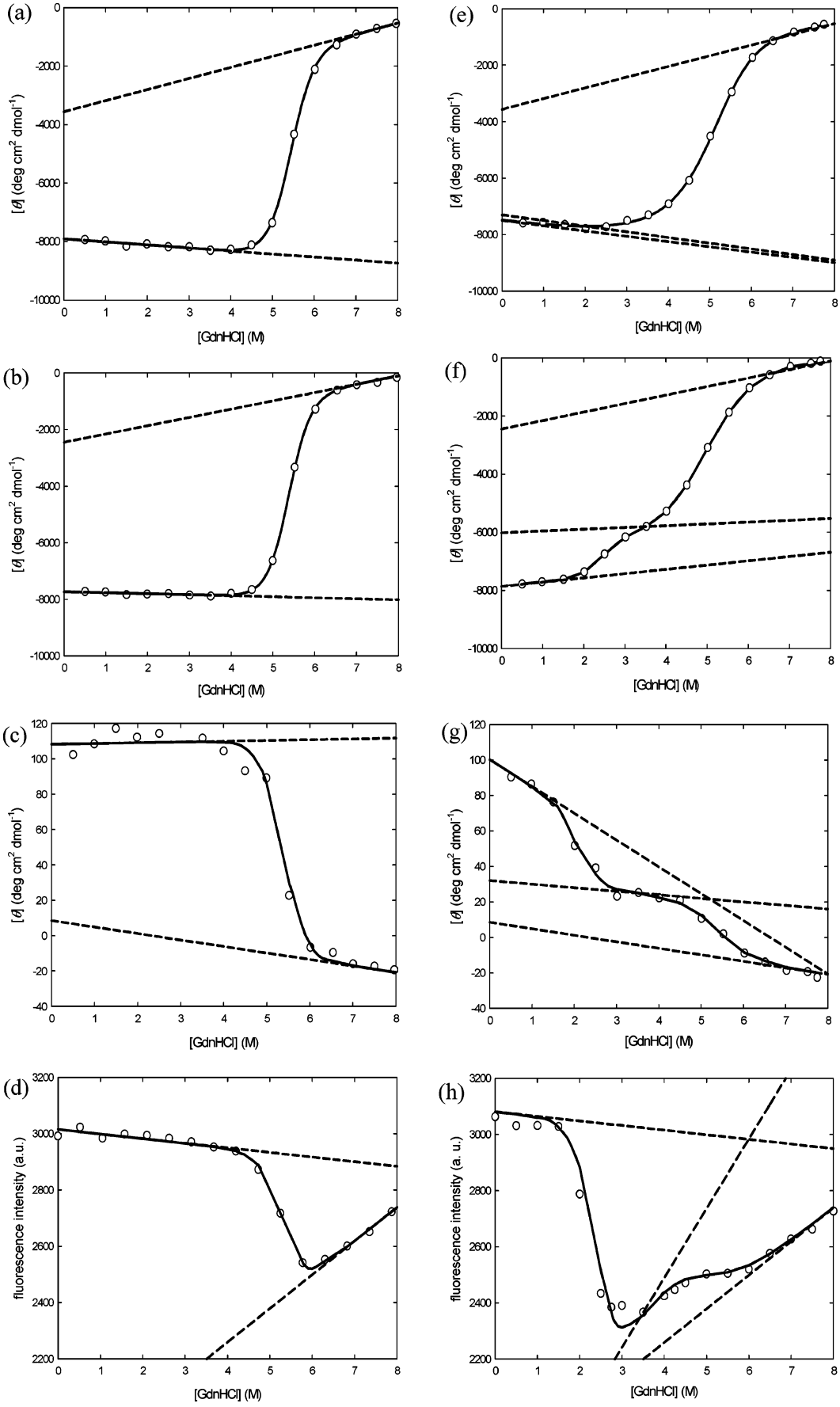

FIGURE 2: GdnHCl-induced equilibrium unfolding transition curves of the holo (left panels) and apo (right panels) N49D variant measured by CD at 222 nm (a and e), 230 nm (b and f), and 295 nm (c and g) and fluorescence emission around 350 nm (d and h) (pH 7.0 and 25 °C). The solid lines represent the theoretical curves based on eqs 2−6. The dashed lines indicate the values of the pure N, I, and U states.

Table 1: Equilibrium Unfolding Parameters of the Holo and Apo N49D Variants (pH 7.0 and 25 °C)

	canine milk lysozyme (recombinant)[a]	apo N49D variant	holo N49D variant (three-state)	holo N49D variant (two-state)	burst-phase intermediate
$\Delta G_{NI}^{H_2O}$ (kcal mol^{-1})	4.41 ± 0.26	5.55 ± 0.38	10.51 ± 0.45		
m_{NI} (kcal mol^{-1} M^{-1})	1.52 ± 0.11	2.27 ± 0.21	2.34 ± 0.33		
$\Delta G_{IU}^{H_2O}$ (kcal mol^{-1})	6.20 ± 0.41	5.15 ± 0.39	5.10 ± 0.60		5.10 ± 0.60
m_{IU} (kcal mol^{-1} M^{-1})	1.26 ± 0.16	1.09 ± 0.23	1.07 ± 0.13		1.07 ± 0.13
$\Delta G_{NU}^{H_2O}$ (kcal mol^{-1})	10.61 ± 0.31	10.70 ± 0.54	15.61 ± 0.75	12.30 ± 0.28	
m_{NU} (kcal mol^{-1} M^{-1})	2.78 ± 0.11	3.36 ± 0.31	3.41 ± 0.35	2.29 ± 0.06	

[a] From Nakao et al. (*16*).

Figure 2 are theoretical curves drawn with the parameter values in Table 1. The theoretical curves agree reasonably well with the experimental data in both the holo and apo forms.

Kinetic Refolding

The observed kinetics for refolding and unfolding were fitted to the following equation:

$$A(t) = A(\infty) + \sum_{i=1}^{n} \Delta A_i \exp(-k_{app,i}t) \quad (7)$$

where $A(t)$ and $A(\infty)$ are the observed signals at time t and the infinite time, respectively, n is the number of exponential phases of the observed kinetics, and ΔA_i and $k_{app,i}$ are the amplitude and the apparent rate constant of the ith phase of the kinetics, respectively.

The refolding reactions of the holo and apo forms were induced by concentration jumps of GdnHCl from 8 M to various final concentrations between 0.7 and 6 M by the stopped-flow mixing technique at pH 7.0 and 25 °C. The kinetics were measured by the time-dependent ellipticity change at 230 nm. For the apo form, we also employed tryptophan fluorescence around 350 nm to measure the refolding kinetics at 1.1 M GdnHCl; these conditions were used in a double-jump stopped-flow unfolding−refolding assay (see below). All of the observed kinetics of refolding were single-exponential ($n = 1$ in eq 7), and the $A(\infty)$ values in the stopped-flow CD measurements were coincident with the values at equilibrium, indicating the reversibility of the unfolding transition. In stopped-flow fluorescence measurements, the fluorometer used was different from that used in the equilibrium measurements, and this prevented us from comparing the $A(\infty)$ and equilibrium values.

(i) Refolding Kinetics of the Holo Form. Figure 3a shows a typical refolding curve of the holo protein at 0.8 M GdnHCl. The nonlinear least-squares fitting of the kinetics to eq 7 ($n = 1$) gave an $A(\infty)$ of −7880 ± 12 deg cm^2 dmol^{-1}, a ΔA of 1030 ± 56 deg cm^2 dmol^{-1} and a k_{app} of 3.0 ± 0.2 s^{-1}; for the single-exponential kinetics, we use the notations ΔA and k_{app} for simplicity by omitting the subscript i in eq 7. These values of k_{app} and ΔA depended on the final refolding condition, and their dependence on c is shown in Figure 4a and b. The k_{app} decreases with increasing c, and the value (0.0071 ± 0.0007 s^{-1}) at 5 M GdnHCl is 3 orders of magnitude smaller than the value at 0.8 M GdnHCl. However, the ΔA gradually increases with c until 4.5 M and then sharply decreases with c above 4.5 M. A comparison between the kinetically observed $A(t)$ extrapolated to zero time (the zero-time ellipticity, $A_{t=0}$) and the equilibrium value for the U state (A_U) indicates that there is missing amplitude, that is, a burst phase in the kinetic refolding of the holo protein. A stable kinetic refolding intermediate thus accumulates within the dead time of the stopped-flow measurement.

(ii) Refolding Kinetics of the Apo Form. Figure 3b shows a typical refolding curve of the apo protein at 0.7 M GdnHCl. The nonlinear least-squares fitting of the kinetics to eq 7 ($n = 1$) gave an $A(\infty)$ of −7790 ± 4 deg cm^2 dmol^{-1}, a ΔA of 1320 ± 17 deg cm^2 dmol^{-1}, and a k_{app} of 2.6 ± 0.1 s^{-1}, which were very close to the corresponding values of the holo protein. In contrast to the refolding reactions of the holo form, however, the kinetics were observed only below 3 M GdnHCl, and there were no observable kinetics above this concentration of GdnHCl. Because the I and the U are mainly populated above 3 M GdnHCl and the population of the N is less than 10%, this observation (of kinetics only below 3 M GdnHC1) suggests that the refolding from the U to the I is too fast to measure by the stopped-flow technique. The dependence of k_{app} and ΔA on c is shown in Figure 4a and b. The k_{app} and ΔA values both decrease with increasing c. The kinetically observed $A_{t=0}$ was much smaller than the equilibrium value (A_U) for the U state, indicating the presence of the burst-phase intermediate in the refolding of the apo protein. This behavior is the same as that observed in the holo protein shown above.

We also carried out kinetic refolding experiments for the apo form using the stopped-flow fluorescence method. Figure 5a shows a typical refolding curve measured by stopped-flow fluorescence. The direction of the fluorescence intensity change agreed with the direction expected from the equilibrium unfolding transition curve (Figure 2h). The nonlinear least-squares fitting of the kinetics to eq 7 ($n = 1$) gave a ΔA of −0.13 ± 0.01 and a k_{app} of 2.4 ± 0.2 s^{-1}. Within experimental error, the k_{app} value was identical to that measured by stopped-flow CD.

(iii) Burst-Phase Intermediate in Kinetic Refolding. From the above results, it is clear that there is a stable burst-phase intermediate in kinetic refolding for both the holo and apo

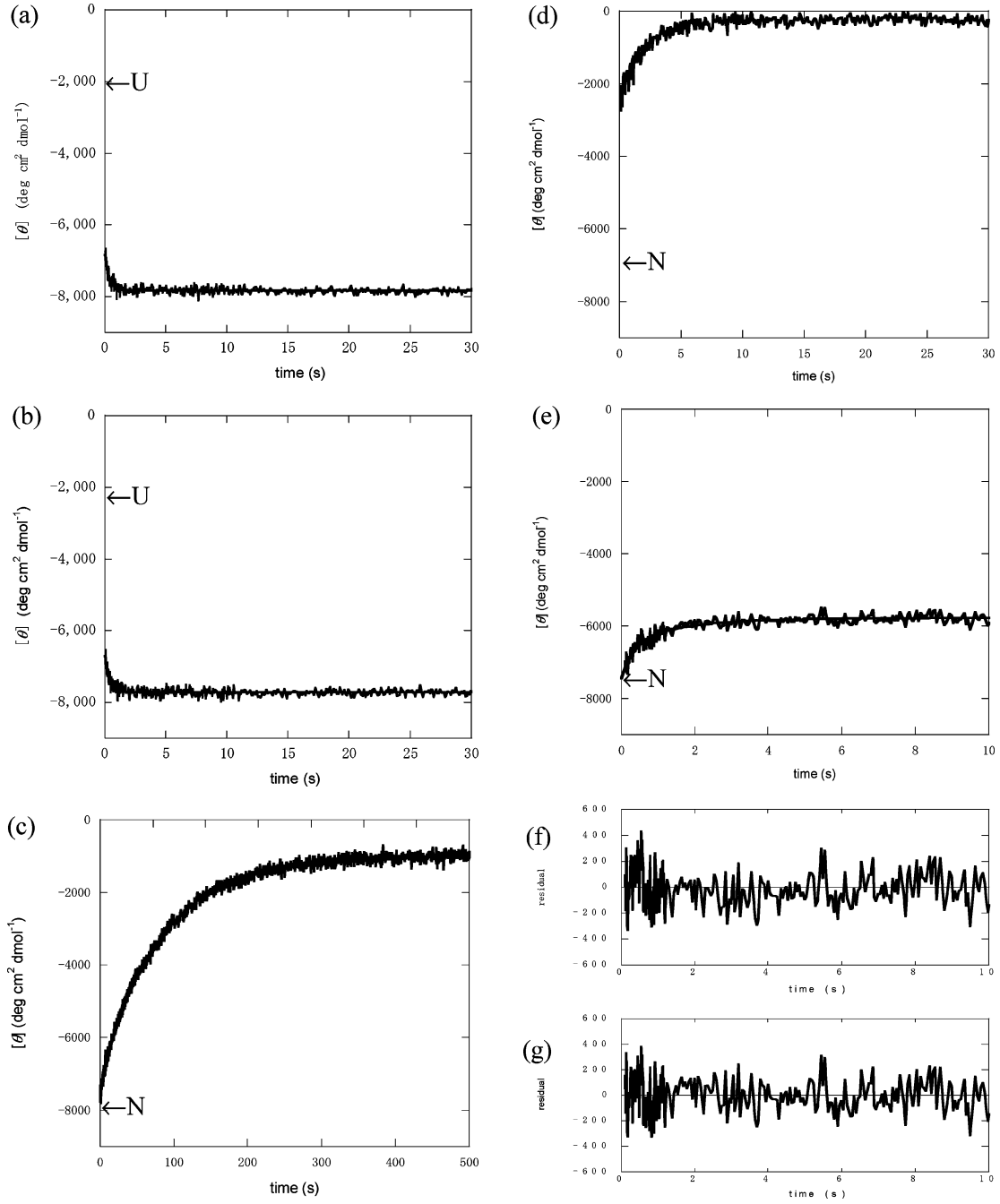

FIGURE 3: Kinetic refolding (a and b) and unfolding (c, d, and e) reaction curves. (a and b) Refolding curves of (a) the holo and (b) apo N49D variants measured by CD at 230 nm. The reaction was initiated by a GdnHCl concentration jump from 8.2 to 0.8 M (the holo form) and from 8.0 to 0.7 M (the apo form). Both curves were well fitted to a single exponential (thick solid line). U denotes the CD values of the holo and apo N49D variants in the U state obtained by extrapolation of the baseline of the U state to 0.8 and 0.7 M GdnHCl, respectively. (c, d, and e) Unfolding curves of the holo (c) and apo-N49D variants (d and e) measured by CD at 230 nm. The reaction was initiated by GdnHCl concentration jumps (c) from 0 to 7.0 M, (d) from 0 to 7.5 M, and (e) from 0 to 3.4 M. The reaction curves in c and d were well fitted to a single exponential, whereas the curve in e was better fitted to double exponentials (eq 7 with $n = 2$). The thick solid lines represent the theoretical curves. N denotes the CD values of the holo and apo N49D variants in the N state obtained by extrapolation of the baseline of the N state. (f and g) Plots of residuals for the reaction curve of e for the single-exponential fitting (f) and the double-exponential fitting (g).

forms of N49D. The refolding reaction is thus represented by the following scheme:

$$U \overset{\text{rapid}}{\rightleftharpoons} I_B \rightarrow N \qquad \text{(scheme 3)}$$

where I_B denotes the burst-phase intermediate.

The dependence of the zero-time ellipticity ($A_{t=0}$) on the GdnHCl concentration (c) gives us the equilibrium unfolding transition curves of I_B (*6*), and Figure 6 shows the unfolding transition curves thus obtained for holo and apo N49D. The unfolding transition curves of the two forms are coincident with each other, indicating that I_B is common between the holo and apo forms. Because the difference in the experimental conditions between the two forms was the presence or absence of Ca^{2+} in solution, the above result means that I_B does not bind to Ca^{2+}.

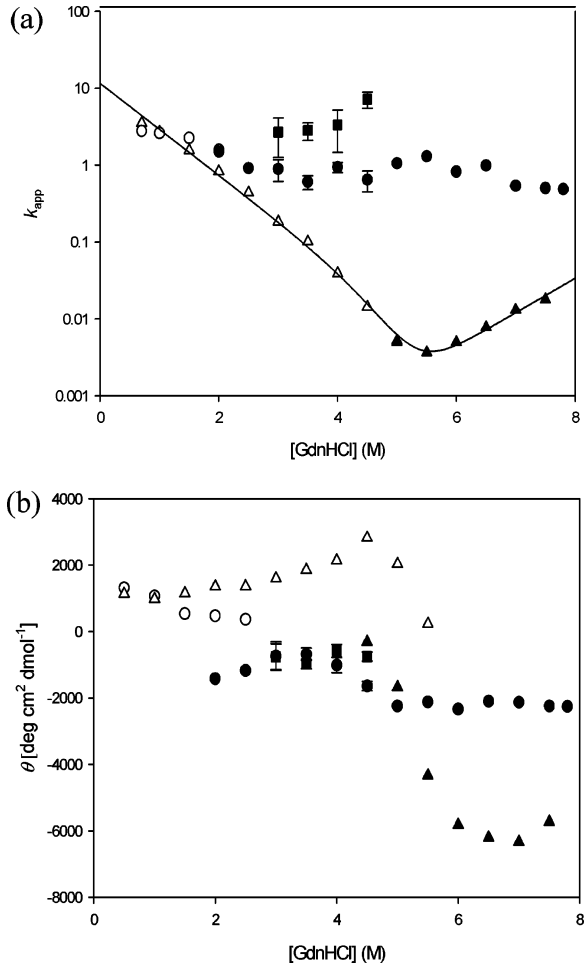

FIGURE 4: GdnHCl concentration dependence of (a) the apparent rate constants and (b) the amplitudes of the kinetic progress curves in the refolding (○, △) and unfolding (●, ▲, ■) reactions of the holo (△, ▲) and apo (○, ● and ■) N49D variants measured by CD (pH 7.0, 25 °C) at 230 nm. The filled circles and squares between 2.5 and 5 M GdnHCl represent the slow and fast phases, respectively, of the double-exponential kinetics observed in the unfolding of the apo form in this concentration range of GdnHCl, and fitting error estimates (standard deviations) are shown for these data. The thick solid line in part a indicates theoretical curves based on eqs 12−14.

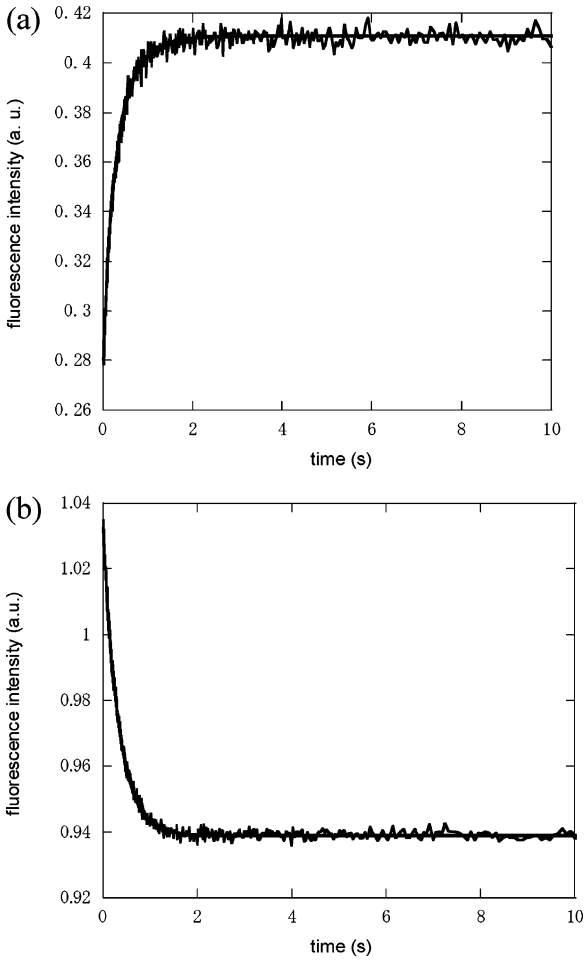

FIGURE 5: (a) Refolding and (b) unfolding reaction curves of the apo N49D variant. Both reactions were monitored by the change in intrinsic tryptophan fluorescence around 350 nm. The reaction was initiated by a GdnHCl concentration jump from 6.6 to 1.1 M (refolding), and from 0 to 6.6 M (unfolding). Both curves were well fitted to a single exponential (thick solid line).

We analyzed the unfolding transition curve of I_B (Figure 6), assuming a two-state transition between I_B and U as follows:

$$I_B \overset{K_{I_BU}}{\rightleftharpoons} U \qquad \text{(scheme 4)}$$

where K_{I_BU} is the equilibrium constant of the unfolding reaction between I_B and U. Because I_B is common between the holo and apo forms, the $A_{t=0}$ values for the two forms were taken together in the analysis. The dependence of $A_{t=0}$ on c is thus given by the following: where A_{I_B} is the ellipticity

$$A_{t=0}(c) = \frac{A_{I_B} + A_U K_{I_BU}}{1 + K_{I_BU}} = \frac{(a_{I_B} + b_{I_B} c) + (a_U + b_U c) K_{I_BU}}{1 + K_{I_BU}} \qquad (8)$$

of the pure I_B state, which was assumed to depend linearly on c, and

$$K_{I_BU} = \exp[-(\Delta G^{H_2O}_{I_BU} - m_{I_BU} c)/RT] \qquad (9)$$

where $\Delta G^{H_2O}_{I_BU}$ and m_{I_BU} are the free energy difference between the I_B and the U at 0 M of c and the cooperativity index of the transition, respectively. The $\Delta G^{H_2O}_{I_BU}$ and m_{I_BU} values thus obtained are 5.10 ± 0.60 kcal mol^{-1} and 1.07 ± 0.13 kcal mol^{-1} M^{-1}, respectively, and these values are identical to the $\Delta G^{H_2O}_{IU}$ and m_{IU} values obtained from the equilibrium unfolding experiments. It is thus concluded that the I_B is identical to the equilibrium intermediate (I).

Kinetic Unfolding

The unfolding reactions of the holo and apo forms were induced by jumping the GdnHCl concentration from 0 M to various final concentrations between 2 and 8 M by the stopped-flow mixing technique at pH 7.0 and 25 °C. The kinetics were measured by the time-dependent ellipticity change at 230 nm. For the apo form, we also employed tryptophan fluorescence around 350 nm to measure the unfolding kinetics at 6.6 M GdnHCl; these conditions were used in a double-jump stopped-flow unfolding−refolding assay (see below). All of the kinetics observed, except for the kinetics of the apo protein between 2.5 and 5 M GdnHCl, were single-exponential and fitted well to eq 7 with $n = 1$. The apo protein kinetics between 2.5 and 5 M GdnHCl were

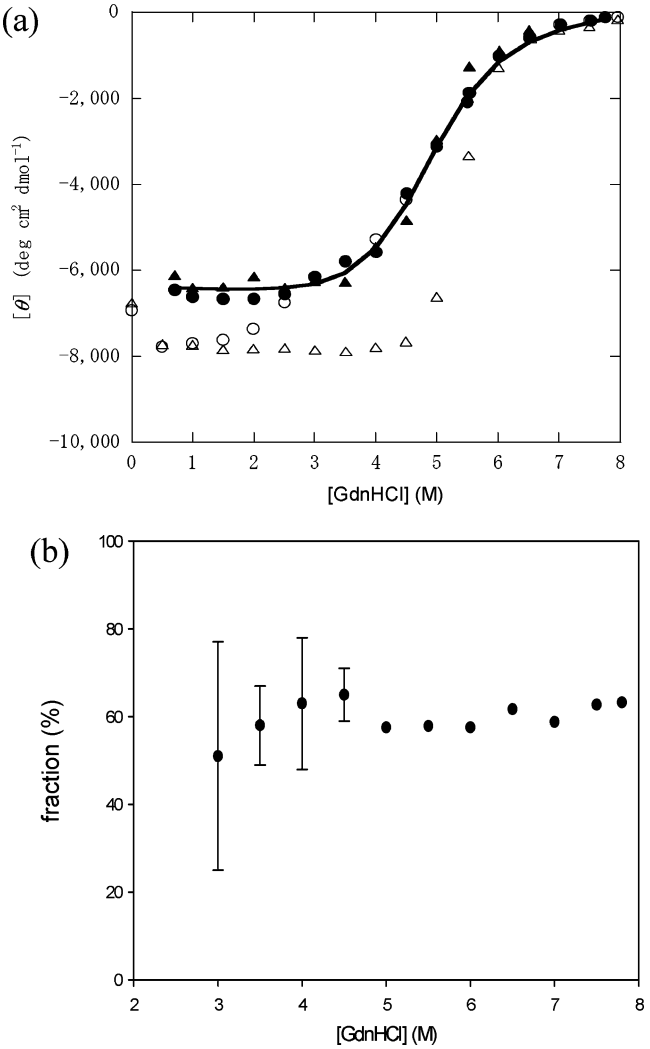

FIGURE 6: (a) GdnHCl-induced equilibrium transition curve (○, △) and the unfolding transition curve of the burst-phase intermediate of the refolding reaction (●, ▲) of the holo (△, ▲) and the apo (○, ●) N49D variants measured by CD at 230 nm. The solid line represents the theoretical curve based on eqs 8 and 9. (b) GdnHCl concentration dependence of the relative amplitude of the burst-phase changes in the unfolding reactions above 5 M GdnHCl of the apo form (●). At a GdnHCl concentration between 2.5 and 5 M, the kinetics were double exponential with no burst phase, and hence, the relative amplitudes of the fast-phase changes of the double-exponential kinetics are shown with error bars. The signal change from the N state to the signal value in the infinite time is defined as 100% of the relative amplitude.

better represented by a double-exponential function and fitted to eq 7 with $n = 2$.

(i) Unfolding Kinetics of the Holo Form. Figure 3c shows a typical unfolding reaction curve of the holo protein at 7.0 M GdnHCl. The nonlinear least-squares fitting of the kinetics to eq 7 ($n = 1$) gave an $A(\infty)$ of -1025 ± 5 deg cm^2 dmol^{-1}, a ΔA of -6337 ± 8 deg cm^2 dmol^{-1}, and a k_{app} of 0.0132 ± 0.0001 s^{-1}. These values of k_{app} and ΔA depended on the final unfolding condition, and their dependence on c is shown in Figure 4a and b. The k_{app} decreases with c below 5.5 M GdnHCl, whereas it increases with c above 5.5 M GdnHCl. The k_{app} value (0.0031 ± 0.0005 s^{-1}) at 5.5 M GdnHCl is thus 1 order of magnitude smaller than the value at 7.5 M GdnHCl. The ΔA sharply decreases with c until 6 M. A comparison between the kinetically observed ΔA and the equilibrium ($A_U - A_N$) values indicates that more than 85% of the ellipticity change expected from the equilibrium unfolding curve (Figure 2b) was observed in the kinetic unfolding.

(ii) Unfolding Kinetics of the Apo Form. Figure 3d shows a typical unfolding reaction curve of the apo protein at 7.5 M GdnHCl, where the observed kinetics were single-exponential. The nonlinear least-squares fitting of the kinetics to eq 7 ($n = 1$) gave an $A(\infty)$ of -239 ± 8 deg cm^2 dmol^{-1}, a ΔA of -2239 ± 17 deg cm^2 dmol^{-1}, and a k_{app} of 0.50 ± 0.01 s^{-1}, which is 29 times larger than that for the holo protein shown above. In contrast to the unfolding reactions of the holo form, the k_{app} and ΔA are both barely dependent on c (Figure 4). Furthermore, the $A_{t=0}$ values obtained by extrapolating the kinetic unfolding curves to zero time were much larger than the equilibrium values (A_N) for the N state, indicating the presence of a burst phase in the unfolding of the apo protein under the same conditions. This behavior is quite different from that of the holo protein shown above.

Figure 3e shows a typical unfolding curve of the apo protein at 3.4 M GdnHCl, where the kinetics were better represented by two exponentials. The nonlinear least-squares fitting of the kinetics to eq 7 ($n = 2$) gave an $A(\infty)$ of -5779 ± 7 deg cm^2 dmol^{-1}, a ΔA_1 of -682 ± 186 deg cm^2 dmol^{-1}, a $k_{app,1}$ of 0.605 ± 0.125 s^{-1}, a ΔA_2 of -975 ± 144 deg cm^2 dmol^{-1}, and a $k_{app,2}$ of 2.832 ± 0.733 s^{-1}. Figure 3f and g show plots of residuals for single-exponential and double-exponential fittings, respectively, and these indicate that the double-exponential fitting is significantly better. The value of $k_{app,1}$ thus obtained is close to the k_{app} values at higher GdnHCl concentrations, where the observed kinetics are single-exponential. The percent amplitude (60%) of the fast phase is coincident with the corresponding amplitude of the burst phase at higher GdnHCl concentrations (Figure 6b), and the $k_{app,2}$ tends to increase with increasing GdnHCl concentration (Figure 4a). These results thus demonstrate that the fast phase corresponds to the burst phase of the kinetics observed at a sufficiently high GdnHCl concentration.

Figure 5b shows an unfolding curve at 6.6 M GdnHCl as measured by stopped-flow fluorescence. The direction of the fluorescence intensity change agreed with the direction expected from the equilibrium unfolding transition curve (Figure 2h). The nonlinear least-squares fitting of the kinetics to eq 7 ($n = 1$) gave a ΔA of 0.095 ± 0.001 and a k_{app} of 1.6 ± 0.06 s^{-1}. Within experimental error, the k_{app} value was identical to that measured by stopped-flow CD.

(iii) Burst Phase in the Unfolding Reaction. There are two possible reaction schemes that explain the observation of the burst phase (or the fast phase when the GdnHCl concentration was between 2.5 and 5 M GdnHCl) in the kinetic unfolding reactions in the apo form measured by stopped-flow CD. One scheme involves the accumulation of the burst-phase unfolding intermediate (X) as shown in scheme 5. In

$$\mathrm{N} \xrightarrow{\text{fast}} \mathrm{X} \xrightarrow{\text{slow}} \mathrm{U} \qquad \text{(scheme 5)}$$

this scheme, we observe the conversion from N to X as the burst phase, and only the conversion from X to U is kinetically accessible. The other scheme assumes heterogeneity in the N state in the apo form. The N state thus consists of slow-unfolding and fast-unfolding species, N_S and N_F, as shown in scheme 6.

$$N_S \overset{\text{slow}}{\rightleftharpoons} N_F \xrightarrow{\text{fast}} U \qquad \text{(scheme 6)}$$

Here, the unfolding from N_F to U is very fast at a GdnHCl concentration above 5 M and occurs within the dead time of stopped-flow measurements, while the interconversion between N_S and N_F occurs slowly, and hence, it is kinetically accessible by the stopped-flow measurement. This scheme thus explains the weak dependence of the unfolding rate constant (k_{app}) on c as well. Because N_S and N_F are both native species, the difference in the surface area accessible to the denaturant GdnHCl must be small, leading to the weak dependence of k_{app} on c. The fraction of the burst-phase amplitude (or the fraction of the fast-phase amplitude at a GdnHCl concentration between 2.5 and 5 M) compared with the total change in the ellipticity expected from the equilibrium unfolding curve was approximately constant (60%) irrespective of c (Figure 6b), and this is also consistent with scheme 6.

(iv) Double-Jump Interrupted Unfolding. To distinguish between schemes 5 and 6, we carried out a double-jump unfolding−refolding experiment in the stopped-flow fluorescence spectrometer, in which sequential double mixing was available. First, the unfolding reaction was induced by a concentration jump of GdnHCl from 0 to 6.6 M (from the N to the U), and the protein was aged under unfolding conditions for a certain period of time (aging time (t_a)). Then the refolding reaction was induced by a concentration jump of GdnHCl from 6.6 to 1.1 M. Figure 7 shows the typical kinetic refolding curve after the second jump to 1.1 M GdnHCl with a t_a of 100 ms. The nonlinear least-squares fitting of the kinetics to eq 7 ($n = 1$) gave a ΔA of -0.035 ± 0.004 and a k_{app} of 2.6 ± 0.1 s^{-1}. The k_{app} is coincident within experimental error with that previously obtained by the single-jump refolding experiment, but the ΔA was 60% of that obtained by the single-jump refolding, considering a difference in the protein concentration between the double-jump and single-jump experiments. We then carried out the double-jump experiment with various t_a values, and the ΔA values thus obtained are plotted as a function of t_a in Figure 8; the fractional ΔA values normalized by the ΔA at $t_a = \infty$ are shown in the Figure.

To investigate whether or not this scheme represents the results of the double-jump experiment, we compared the data in Figure 8 with the theoretical curve based on scheme 6. According to scheme 6, the fractional amplitude (F) shown in Figure 8 is related to the fractional amplitude (F_{burst}) of the burst phase and the fractional amplitude (F_{obs}) of the single-exponential kinetic phase in the unfolding reaction observed by the stopped-flow CD, and this relation is given by the following equation:

$$F(t_a) = F_{burst} + F_{obs}\,[1 - \exp(-k_{app}t_a)] \qquad (10)$$

Here, F_{burst} and F_{obs} are normalized by the total ellipticity change from U to N, 0.6 and 0.4, respectively, and k_{app} is the apparent rate constant of unfolding under first-jump unfolding conditions (6.6 M GdnHCl) ($k_{app} = 1.6$ s^{-1}). The theoretical curve drawn with these parameter values shows excellent agreement with the experimental data in Figure 8, strongly demonstrating that scheme 6 represents the unfolding of the apo protein.

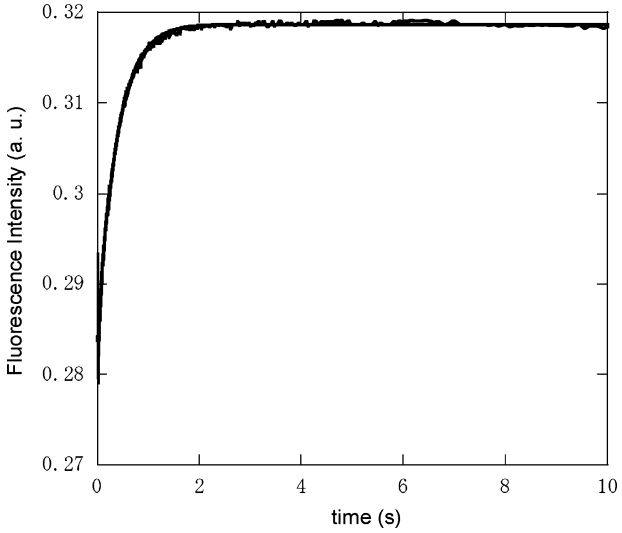

FIGURE 7: Kinetic refolding curve in the interrupted unfolding experiment of the apo N49D variant. Reaction was monitored by the change in intrinsic tryptophan fluorescence. The curve was well fitted to a single exponential (thick solid line).

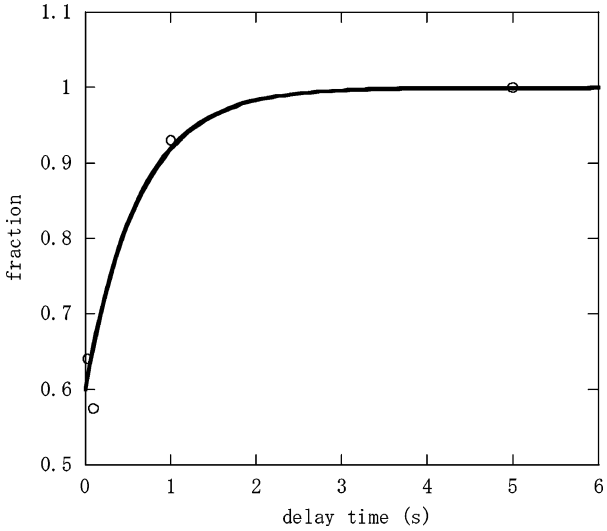

FIGURE 8: Normalized amplitude of the refolding reaction curves in the interrupted unfolding experiments. The amplitude is normalized by the amplitude of the refolding reaction curve in the single-jump experiment. The thick solid line is a theoretical curve based on eq 10.

DISCUSSION

Members of the lysozyme/α-LA family are known to exhibit the MG state as an equilibrium unfolding intermediate and a kinetic folding intermediate. Among the intermediates assumed by the members, the MG state of canine milk lysozyme is the most stable and most native-like (*15*, *16*). The presence of residual specific tertiary packing of some aromatic residues in the MG state is peculiar to canine and equine milk lysozymes, whereas in other proteins, the specific tertiary interactions of side chains are almost fully disrupted in the MG state. It is thus intriguing to address the question of how such a high stability and the residual native-like tertiary structure of the MG state affect the canine protein-folding mechanism. The results of the present study indicate that both the holo and apo proteins assume the same burst-phase kinetic folding intermediate and that this kinetic intermediate is identical to the equilibrium MG state observed

Table 2: Kinetic and Equilibrium *m* Values and Relative Degrees of Organization in the I and Transition States (pH 7.0 and 25 °C)

	$m_{u‡}$ (kcal mol^{-1} M^{-1})	m_{IU} (kcal mol^{-1} M^{-1})	m_{NU} (kcal mol^{-1} M^{-1})	α_I (%)	$\alpha_‡$ (%)
canine milk lysozyme	0.48 ± 0.07	1.09 ± 0.23	3.36 ± 0.10	32 ± 7	86 ± 1
equine lysozyme[a]	0.53 ± 0.03	1.13 ± 0.19	3.13 ± 0.15	36 ± 6	83 ± 1
bovine α-LA[b]	1.14 ± 0.04	0.75	2.39	30	52

[a] From Mizuguchi et al. (*27*). [b] From Kuwajima et al. (*24*) and Ikeguchi et al. (*28*).

in the unfolding of the apo protein. These results are thus very analogous to those previously observed in the α-LA and another Ca^{2+}-binding lysozyme (equine milk lysozyme). The $\Delta G_{NU}^{H_2O}$ and $\Delta G_{IU}^{H_2O}$ values are, however, all larger than the corresponding values of the other members of the lysozyme/α-LA family, and the m_{IU} value is also larger and equal to the value observed previously for equine milk lysozyme, which also exhibits the stable MG state.

We also studied the effect of Ca^{2+} on the folding and unfolding behavior of canine milk lysozyme. The coincidence of the unfolding transition curves of the MG state between the apo and holo forms indicates that the MG state is not stabilized by and hence not bound to Ca^{2+} (Figure 6). Furthermore, the presence of 10 mM Ca^{2+} affected only the unfolding rate constant; it remarkably decelerated the unfolding rate but did not affect the refolding rate (Figure 4a). This result thus suggests that the Ca^{2+}-binding site has not yet been organized in the transition state located between the I and N states. This is apparently in contrast with the previous observation reported for α-LA, in which the Ca^{2+}-binding site is organized in the transition state (*24*, *25*). Finally, the results of the kinetic unfolding reactions and the double-jump interrupted unfolding reactions have revealed that the apo protein includes two native species, which slowly interconvert with a k_{app} on the order of 1 s^{-1}.

We now further discuss the role of the MG state thus observed, the effect of Ca^{2+} on the equilibrium unfolding and folding kinetics of the protein, and finally the heterogeneity of the N state of the protein's apo form.

Role of the MG Intermediate in the Folding of Canine Milk Lysozyme. The presence of native-like tertiary packing of some side chains in the MG state would lead us to expect that the formation of the MG state of canine milk lysozyme might be slower than those of the classical MG states of other proteins. Rather surprisingly, however, the present results have revealed that the MG state of the canine protein is formed within the dead time of the stopped-flow apparatus. Because the dead time of the apparatus employed was 3.5 ms for the stopped-flow fluorescence and 25 ms for the stopped-flow CD, we need to employ an even faster reaction technique to investigate whether or not the MG state of the canine protein is formed more slowly than the MG states of the other proteins.

The rapid pre-equilibrium between the unfolded state (U) and the MG folding intermediate (I) may affect the dependence of the apparent rate constant k_{app} of folding on GdnHCl concentration *c*, and this behavior is known as the rollover on the folding limb of a chevron plot. Such a rollover is clearly seen in the chevron plot of the holo form of the protein (Figure 4a). Assuming an on-pathway model for folding, the reaction scheme is given by the following:

$$U \overset{1/K_{IU}}{\rightleftharpoons} I \underset{k_u}{\overset{k_f}{\rightleftharpoons}} N \qquad \text{(scheme 7)}$$

where k_f and k_u are the microscopic rate constants of folding and unfolding, respectively. The k_{app} value is thus given by the following equation:

$$k_{app} = k_u + \frac{k_f}{1 + K_{IU}} \tag{11}$$

To simplify the following analysis, we assume the linear dependence of ln k_f and ln k_u on *c* as follows (*26*):

$$\ln k_f = \ln k_f^{H_2O} + \frac{m_f^{‡} c}{RT} \tag{12}$$

$$\ln k_u = \ln k_u^{H_2O} + \frac{m_u^{‡} c}{RT} \tag{13}$$

where $k_f^{H_2O}$ and $k_u^{H_2O}$ are the k_f and k_u at 0 M GdnHCl, and $m_f^{‡}$ and $m_u^{‡}$ are the *m* values for the activation processes from I and from N to the transition state, respectively. We could reasonably fit the chevron plot to these equations with the parameters ($\Delta G_{IU}^{H_2O}$ and m_{IU}) obtained from the equilibrium unfolding experiments (Figure 4a). The result is thus consistent with the sequential folding mechanism with the MG state as an on-pathway folding intermediate (scheme 7).

Table 2 summarizes the equilibrium and kinetic *m* values (m_{NU}, m_{IU}, $m_u^{‡}$) from which we can estimate the relative degrees of structural organization, $\alpha_‡$ and α_I, in the transition state of folding and in the MG folding intermediate, respectively. The $\alpha_‡$ and α_I are thus given by the following:

$$\alpha_‡ = 1 - \frac{m_u^{‡}}{m_{NU}} \tag{14}$$

$$\alpha_I = \frac{m_{IU}}{m_{NU}} \tag{15}$$

The $\alpha_‡$ value was 86 ± 1% for the holo form of canine milk lysozyme, and it was 52 and 83 ± 1% for bovine α-LA (*24*) and equine milk lysozyme (*27*), respectively, indicating that the transition state of canine milk lysozyme is the most highly organized. The α_I value was estimated at 32 ± 7% for canine milk lysozyme. The corresponding values for α-LA and equine milk lysozyme were 30 (*28*) and 36 ± 6% (*27*), respectively, and hence, the α_I values of the three proteins fell within the same range. Because $\alpha_‡ > \alpha_I$, the relative degree of structural organization progressively increases during the folding from the U state via the MG

intermediate and the transition state to the N state in these proteins. This finding is consistent with the sequential on-pathway model of protein folding, in which the structure organized in the MG intermediate is retained during the subsequent process to the N state.

For the apo form, the presence of the different native species (N_S and N_F) has made the evaluation of $\alpha_\ddagger$ difficult, but the fast-phase rate constant of unfolding from N_F to U, shows linear dependence on *c*, similar to that observed in the unfolding of the holo form (Figure 4a). A similar $\alpha_\ddagger$ value may thus be expected for the apo form as well.

Effects of Ca^{2+} on the Equilibrium Unfolding of Canine Milk Lysozyme. The equilibrium unfolding of the apo form was represented by a three-state model with the MG state as an unfolding intermediate, and the population of the MG state was as large as 91% at 3.4 M GdnHCl. For the holo form of the protein, however, we analyzed equilibrium unfolding on the basis of a two-state model in which only the N and U states were populated during the unfolding transition. In fact, the apparent unfolding transition curves measured by different spectral probes (far-UV CD, near-UV CD, and tryptophan fluorescence) were approximately coincident with each other (Figure 2a−d). Stabilization of the N state by the bound Ca^{2+} in the holo protein made the fraction of the MG state much smaller than those of the N and U states. Hence, the observed unfolding transition might obey the two-state mechanism.

However, the m_{NU} value (2.29 kcal mol^{-1} M^{-1}) of the holo form evaluated by the two-state model was significantly smaller than the corresponding value (3.36 kcal mol^{-1} M^{-1}) of the apo form evaluated by the three-state model (Table 1). This suggests that the unfolding of the holo form should also be represented by the three-state model. Therefore, we re-analyzed the equilibrium unfolding data (Figure 2a−d) of the holo form by the three-state model using eqs 4−6. In this analysis, however, we had to obtain the fraction of the MG intermediate (I) or the equilibrium constant K_{IU} in another way because the fraction or K_{IU} was scarcely apparent in the equilibrium unfolding curves. We thus used the unfolding parameters ($\Delta G_{IU}^{H_2O}$ and m_{IU}) for the burst-phase MG intermediate of refolding to obtain the K_{IU} value at a given *c* (Table 1). We then performed global fitting in which the four unfolding transition curves of Figure 2a−d were fitted simultaneously with the two global fitting parameters of $\Delta G_{NI}^{H_2O}$ and m_{NI}. The thermodynamic parameters thus obtained are also summarized in Table 1. According to these parameter values, the maximum fraction of the equilibrium MG intermediate is 0.18 at 4.6 M GdnHCl. The m_{NU} value (3.41 kcal mol^{-1} M^{-1}) of the holo form is now in excellent agreement with that of the apo form (Table 1). Therefore, the equilibrium unfolding of the holo form is better represented by the three-state mechanism.

The equilibrium unfolding of canine milk lysozyme and equine milk lysozyme is represented by the three-state mechanism in both the holo and apo forms. In contrast, the equilibrium unfolding of bovine α-LA is represented by the three-state mechanism in the apo form and by the two-state mechanism in the holo form. This difference can be explained by the difference in their X-ray crystallographic structures. In the canine and equine proteins, the groups on the face opposite the Ca^{2+}-binding site in a cleft region located at the interface between the α- and *β*-domains are loosely packed, and this divides each protein into two well-defined densely packed clusters (*21*, *24*, *29*). Thus, the two domains independently unfold in the equilibrium unfolding of these proteins in the apo form, and this behavior remains to some extent in the holo form as well (*24*). In bovine α-LA, the corresponding groups at the interface are also loosely packed in the apo form, which similarly divides the protein into two well-defined densely packed clusters (*30*). In the holo form of α-LA, however, Ca^{2+} binding has induced not only small conformational changes of residues around the Ca^{2+}-binding site but also large conformational changes of the groups at the interface, resulting in the well-packed interface region and the reinforced interactions between the two domains (*30*). Therefore, the two domains of the protein are integrated into one large cluster and hence unfold in a cooperative manner. As found in the holo form of α-LA, the equilibrium unfolding of hen egg white lysozyme is represented by the two-state mechanism (*31*, *32*), and this is again consistent with its structure, in which the interface between the α- and *β*-domains of this protein is densely packed (*33*). These packing differences at the domain interface thus reasonably explain the differences in the unfolding behavior between these proteins.

Effects of Ca^{2+} on the Folding and Unfolding Kinetics of Canine Milk Lysozyme. From the change in the rate constant of folding (or unfolding) caused by Ca^{2+} binding to the protein, that is, from the difference in the rate constant between the holo and apo forms of the protein, we can obtain a Φ-value of protein folding at the Ca^{2+}-binding site (*24*, *34*). Because the Ca^{2+} binding itself is assumed to be much faster than folding and unfolding reactions, any change in the rate constant of folding (or unfolding) may reflect the organization (or disruption) of the Ca^{2+}-binding site during the activation process from U (or N) to the transition state. The Φ-value is thus calculated using the following equation:

$$\Phi = 1 - \frac{RT \ln \dfrac{k_u^{holo}(c_M^{apo})}{k_u^{apo}(c_M^{apo})}}{\Delta\Delta G_{NU}(c_M^{apo})} \qquad (16)$$

where $k_u^{holo}(c_M^{apo})$ and $k_u^{apo}(c_M^{apo})$ are the unfolding rate constants of the holo and apo forms, respectively, at the midpoint denaturant concentration (c_M^{apo}) for the unfolding of the apo form, and c_M^{apo} is 2.4 M. Here, we calculated the Φ-value at c_M^{apo} because long extrapolation of the thermodynamic and kinetic parameters to 0 M GdnHCl could have caused a large error in estimating the Φ-value. From Figure 4a, we estimated $k_u^{apo}(c_M^{apo})$ at 0.9 s^{-1}, whereas $k_u^{holo}(c_M^{apo})$ was estimated at 2.8×10^{-4} s^{-1} from eq 13 using the values shown in Table 2. The Φ-value is thus −0.15 for canine milk lysozyme and is much smaller than the corresponding value (0.76) for bovine α-LA (*24*). Therefore, the Ca^{2+}-binding site has not yet been organized in the transition state of canine milk lysozyme, and this is in contrast to the known results for bovine and goat α-LA in which the site is organized in the transition state of folding (*24*, *25*). These results are thus rather surprising because the relative degree of structural organization ($\alpha_\ddagger$) of the transition state has been shown to be much larger (86%) for canine milk lysozyme than for bovine and goat α-LA (52%) (*24*, *25*).

Folding Mechanisms of Canine Milk Lysozyme and Bovine α-LA. The absence of an organized structure around the Ca^{2+}-binding site in the transition state of folding in canine milk lysozyme, in spite of its presence in bovine α-LA, has a significant implication concerning the folding mechanisms of the lysozyme/α-LA family. For bovine and goat α-LA, the structure organized in the transition state is very localized in a region that involves the Ca^{2+}-binding site and the C-helix, and hence, this region must be the folding initiation site in these proteins (*24*, *25*). The folding initiation site of canine milk lysozyme, however, must be located at a place other than the Ca^{2+}-binding site, indicating that the folding pathways must be different between canine milk lysozyme and α-LA. These results thus provide an example in which proteins that are very homologous to each other exhibit different folding initiation sites and hence different folding pathways; the homology between canine milk lysozyme and bovine α-LA is 42%. Other examples in which homologous proteins can adopt different folding pathways include apomyoglobin and leghemoglobin (*35*).

From the H/D-exchange study of the MG state at pH 2.0 and the N state at pH 4.5 of canine milk lysozyme, the A- and B-helices are stabilized in the MG state of this protein. In contrast, the C-helix is stabilized in the MG state of bovine (*36*) and goat α-LA (Nakamura, T., et al., unpublished results). Therefore, the structures stabilized in the MG state are also different between canine milk lysozyme and bovine (and goat) α-LA, and these differences are consistent with the differences in the transition-state structure between the proteins. The C-helix that is stabilized in α-LA is very close to the Ca^{2+}-binding site, whereas the A- and B-helices that are stabilized in canine milk lysozyme are away from the Ca^{2+}-binding site. These results thus suggest that the folding initiation site of canine milk lysozyme may be located in a region that involves A- and B-helices.

Heterogeneity of the Native State. Although the holo form of canine milk lysozyme assumes only one native species, its apo form assumes at least two native species, which interconvert with a rate constant on the order of 1 s^{-1}. Such multiple native species were also observed for adenylate kinase (AK) (*37*), calbindin D_{9k} (*38*), SecA (*39*), dihydrofolate reductase (DHFR) (*40*), and staphylococcal nuclease (SNase) (*41*). In the equilibrium unfolding and kinetic refolding experiments of canine milk lysozyme, no signals indicating the multiple native species were observed, suggesting that N_S and N_F are not distinguishable by CD or fluorescence spectroscopy. The fractions of N_S and N_F under native conditions are 0.4 and 0.6, respectively (Figure 6b), indicating that the thermodynamic stabilities (free energies) of N_S and N_F are very close to each other, and the m_{NU} values for the apo and holo forms are identical (Table 1), indicating that the native-state heterogeneity of the apo form did not bring a significant change in solvent accessibility of the native structure. Similar results were also observed in DHFR and SecA, in which the multiple native species are converted into each other with little change in their conformations, as determined by small changes in solvent accessibility and optical properties.

One question is the origin of heterogeneity in native apo canine milk lysozyme. The heterogeneity of native AK, calbindin D_{9k}, and SNase is known to result from the cis−trans isomerization of a peptidyl-prolyl bond, and the rate constant of the interconversion between the multiple native species of these proteins is consistent with the rate constant of the prolyl isomerization (<0.1 s^{-1}) (*37*, *38*, *41*). For canine milk lysozyme, however, the rate constant of the interconversion may be too fast to be rate-limited by the proline isomerization. The interconversion between the multiple native species of DHFR is also fast, with a rate constant larger than 1 s^{-1}, and the heterogeneity of native DHFR is not localized but rather is caused by different docking modes between two domains of the protein (*42*). The heterogeneity of native canine milk lysozyme might also be due to a difference in the interaction between the α- and *β*-domains of the protein or to a local structural difference within each domain between the N_F and N_S species. Although there are still some questions about the origin of the native-state heterogeneity of canine milk lysozyme, the present study provides the first such observation in the lysozyme/α-LA family. Further elucidation of the origin of native-state heterogeneity should be an important subject for future studies of this protein family.

Another question is the origin of the difference between the holo and apo forms of canine milk lysozyme with respect to the homogeneity or heterogeneity of the N state. One possible explanation is that the binding constant of the protein with the Ca^{2+} is very different between the two native species so that only one of the two native species is bound to Ca^{2+} and stabilized. This situation was observed in AK, in which the two native species have different affinities for its substrate, and substrate binding increases the population of one of the two native species (*43*).

ACKNOWLEDGMENT

We are grateful to Dr. M. Arai (National Institute of Advanced Industrial Science and Technology (AIST)) and Dr. M. Nakao (Yokohama City University) for invaluable advice. We also thank an anonymous referee of the present article for his/her valuable comments concerning the kinetics of the apo protein.

REFERENCES

1. Anfinsen, C. B. (1973) Principles that govern the folding of protein chains, *Science 181*, 223−230.
2. Kuwajima, K. (1989) The molten globule state as a clue of understanding the folding and cooperativity of globular-protein structure, *Proteins 6*, 87−103.
3. Ptitsyn, O. B. (1995) Molten globule and protein folding, *Adv. Protein Chem. 47*, 83−229.
4. Arai, M., and Kuwajima, K. (2000) Role of the molten globule state in protein folding, *Adv. Protein Chem. 53*, 209−282.
5. Jackson, S. E. (1998) How do small single-domain proteins fold? *Folding Des. 3*, R81−R91.
6. Arai, M., and Kuwajima, K. (1996) Rapid formation of a molten globule intermediate in refolding of α-lactalbumin, *Folding Des. 1*, 275−287.
7. Jennings, P. A., and Wright, P. E. (1993) Formation of a molten globule intermediate early in the kinetic folding pathway of apomyoglobin, *Science 262*, 892−896.
8. Raschke, T. M., Kho. J., and Marqusee, S. (1999) Confirmation of the hierarchical folding of RNase H: a protein engineering study, *Nat. Struct. Biol. 6*, 825−831.
9. Pervaiz, S., and Brew, K. (1986) Purification and characterization of the major whey proteins from the milks of the bottlenose dolphin (*Tursiops truncates*), the florida manatee (*Trichechus manatus latirostris*), and the beagle (*Canis familiaris*), *Arch. Biochem. Biophys. 246*, 846−854.

10. Kikuchi, M., Kawano, K., and Nitta, K. (1998) Calcium-binding and structural stability of echidna and canine milk lysozyme, *Protein Sci. 7*, 2150−2155.
11. Nitta, K., and Sugai, S. (1989) The evolution of lysozyme and α-lactalbumin, *Eur. J. Biochem. 182*, 111−118.
12. Grobler, J. A., Rao, K. R., Pervaiz, S., and Brew, K. (1994) Sequences of two highly divergent canine type c lysozymes: implications for the evolutionary origins of the lysozyme/α-lactalbumin superfamily, *Arch. Biochem. Biophys. 313*, 360−366.
13. Koshiba, T., Yao, M., Kobashigawa, Y., Demura, M., Nakagawa, A., Tanaka, I., Kuwajima, K., and Nitta, K. (2000) Structure and thermodynamics of the extraordinarily stable molten globule state of canine milk lysozyme, *Biochemistry 39*, 3248−3257.
14. Koshiba, T, Hayashi, T., Ishido, M., Kumagai, I., Ikura, T., Kawano, K., and Nitta, K., and Kuwajima, K. (1999) Expression of a synthetic gene encoding canine milk lysozyme in Escherichia coli and characterization of the expressed protein, *Protein Eng. 12*, 429−435.
15. Kobashigawa, Y., Demura, M., Koshiba, T., Kumaki, Y., Kuwajima, K., and Nitta, K. (2000) Hydrogen exchange study of canine milk lysozyme: stabilization mechanism of the molten globule, *Proteins 40*, 579−589.
16. Nakao, M., Arai, M., Koshiba, T., Nitta, K., and Kuwajima, K. (2003) Folding mechanism of canine milk lysozyme studied by circular dichroism and fluorescence spectroscopy, *Spectroscopy 17*, 183−193.
17. Van Dael, H., Haezebrouck, P., and Joniau, M. (2003) Equilibrium and kinetic studies on folding of canine milk lysozyme, *Protein Sci. 12*, 609−619.
18. Nakao, M., Maki, K., Arai, M., Koshiba, T., Nitta, K., and Kuwajima, K. (2005) Characterization of kinetic folding intermediates of recombinant canine milk lysozyme by stopped-flow circular dichroism, *Biochemistry 44*, 6685−6692.
19. Takano, K., Tsuchimori, K., Yamagata, Y., and Yutani, K. (1999) Effect of foreign N-terminal residues on the conformational stability of human lysozyme, *Eur. J. Biochem. 266*, 675−682.
20. Chaudhuri, T. K., Horii, K., Yoda, T., Arai, M., Nagata, S., Terada, T. P., Uchiyama, H., Ikura, T., Tsumoto, K., Kataoka, H., Matsushima, M., Kuwajima, K., and Kumagai, I. (1999) Effect of the extra N-terminal methionine residue on the stability and folding of recombinant α-lactalbumin expressed in *Escherichia coli*, *J. Mol. Biol. 285*, 1179−1194.
21. Akieda, D., Yasui, M., Nonaka, Y., Watanabe, M., Yao, M., Watanabe, N., Tanaka, I., Aizawa, T., Nitta, K., Demura, M., and Kawano, K. Construction of an expression system of canine milk lysozyme in the methylotrophic yeast *Pichia pastoris*, unpublished work.
22. Pace, C. N. (1986) Determination and analysis of urea and guanidine hydrochloride denaturation curves, *Methods Enzymol. 131*, 266−280.
23. Santoro, M. M., and Bolen, D. W. (1992) A test of the linear extrapolation of unfolding free energy changes over an extended denaturant concentration range, *Biochemistry 31*, 4901−4907.
24. Kuwajima, K., Mitani, M., and Sugai, S. (1989) Characterization of the critical state in protein folding: Effects of guanidine hydrochloride and specific Ca^{2+} binding on the folding kinetics of α-lactalbumin, *J. Mol. Biol. 206*, 547−561.
25. Saeki, K., Arai, M., Yoda, T., Nakao, M., and Kuwajima, K. (2004) Localized nature of the transition-state structure in goat α-lactalbumin folding, *J. Mol. Biol. 341*, 589−604.
26. Tanford, C. (1970) Protein denaturation, *Adv. Protein Chem. 24*, 1−95.
27. Mizuguchi, M., Arai, M., Ke, Y., Nitta, K., and Kuwajima, K. (1998) Equilibrium and kinetics of the folding of equine milk lysozyme studied by circular dichroism spectroscopy, *J. Mol. Biol. 283*, 265−277.
28. Ikeguchi, M., Kuwajima, K., Mitani, M., and Sugai, S. (1986) Ca^{2+}-induced alternation in the unfolding behavior of α-lactalbumin, *J. Biochem. 99*, 1191−1201.
29. Tsuge, H., Ago, H., Noma, M., Nitta, K., Sugai, S., and Miyano, M. (1992) Crystallographic studies of a calcium binding lysozyme from equine milk at 2.5 Å resolution, *J. Biochem. (Tokyo), 111*, 141−143.
30. Chrysina, E. D., Brew, K., and Acharya, K. R. (2000) Crystal structures of apo- and holo-bovine α-lactalbumin at 22-Å resolution reveal an effect of calcium on inter-lobe interactions, *J. Biol. Chem. 47*, 37021−37029.
31. Aune, K. C., and Tanford, C. (1969) Thermodynamics of the denaturation of lysozyme by guanidine hydrochloride. II. Dependence on denaturant concentration at 25 degrees, *Biochemistry 8*, 4586−4590.
32. Pfeil, W., and Privalov, P. L. (1976) Thermodynamic investigations of proteins. 1. Standard functions for proteins with lysozyme as an example, *Biophys. Chem. 4*, 23−32.
33. Griko, Y. V., Freire, E., Privalov, G., Van Dael, H., and Privalov, P. L. (1995) The unfolding thermodynamics of c-type lysozymes: A calorimetric study of the heat denaturation of equine lysozyme, *J. Mol. Biol. 252*, 447−259.
34. Matouschek, A., Kellis, J. T., Serrano, L., and Fersht, A. R. (1989) Mapping the transition state and pathway of protein folding by protein engineering, *Nature, 340*, 122−126.
35. Nishimura, C., Prytulla, S., Dyson, H. J., and Wright, P. E. (2000) Conservation of folding pathways in evolutionarily distant globin sequences, *Nat. Struct. Biol. 7*, 679−686.
36. Forge, V., Wijesinha, R. T., Balbach, J., Brew, K., Robinson, C. V., Redfield, C., and Dobson, C. M. (1999) Rapid collapse and slow structural reorganization during the refolding of bovine alpha-lactalbumin, *J. Mol. Biol. 288*, 673−688.
37. Zhang, H. J., Sheng, X. R., Niu, W. D., Pan, X. M., and Zhou, J. M. (1998) Evidence for at least two native forms of rabbit muscle adenylate kinase in equilibrium in aqueous solution, *J. Biol. Chem. 13*, 7448−7456.
38. Chazin, W. J., Kördel, J., Drakenberg, T., Thulin, E., Hoffman, T., and Forsën, S. (1989) Proline isomerism leads to multiple folded conformations of calbindin D_{9k}: Direct evidence from two-dimensional ^{1}H NMR spectroscopy, *Proc. Natl. Acad. Sci. U.S.A. 86*, 2195−2198.
39. Doyle, S. M., Bilsel, O., and Teschke, C. M. (2004) SecA folding kinetics: A large dimeric protein rapidly forms multiple native states, *J. Mol. Biol. 341*, 199−214.
40. Jennings, P. A., Finn, B. E., and Matthews, C. R. (1993) A reexamination of the folding mechanism of dihydrofolate reductase from *Escherichia coli:* Verification and refinement of a four-channel model, *Biochemistry 32*, 3783−3789.
41. Evance, P. A., Dobson, C. M., Kauz, R. A., Hatfull, G., and Fox, R. O. (1987) Proline isomerism in staphylococcal nuclease characterized by NMR and site directed mutagenesis, *Nature, 329*, 266−268.
42. Ionescu, R. M., Smith, V. F., O'Neil, J. C., Jr., and Matthews, C. R. (2000) Multistate equilibrium unfolding of *Escherichia coli* dihydrofolate reductase: thermodynamic and spectroscopic description of the native, intermediate, and unfolded ensembles, *Biochemistry, 39*, 9540−9550.
43. Sheng, X. R., Li, X., and Pan, X. M. (1999) An iso-random Bi Bi mechanism for adenylate kinase, *J. Biol. Chem. 274*, 22238−22242.

BI602464V